

Evaluation of a Spline-Based Parameterization Scheme for Phase-Only Antenna Pattern Synthesis

Reece J. Reinke 

Advanced Radar Research Center
The University of Oklahoma
Norman Oklahoma, USA
reecereinke@ou.edu

David Schwartzman 

Advanced Radar Research Center
School of Meteorology
The University of Oklahoma
Norman Oklahoma, USA
dschvart@ou.edu

Feng Nai 

CIWRO/NSSL
The University of Oklahoma
Norman Oklahoma, USA
feng.nai@noaa.gov

Tian-You Yu 

Advanced Radar Research Center
School of Electrical and Computer Eng.
The University of Oklahoma
Norman Oklahoma, USA
tyu@ou.edu

Jorge Salazar-Cerreño 

Advanced Radar Research Center
School of Electrical and Computer Eng.
The University of Oklahoma
Norman Oklahoma, USA
salazar@ou.edu

Robert D. Palmer 

Advanced Radar Research Center
School of Meteorology
The University of Oklahoma
Norman Oklahoma, USA
rpalmer@ou.edu

Abstract—Phased Array Radars (PAR) are rapidly becoming the future for weather observations. The National Oceanic and Atmospheric Administration (NOAA) has identified PARs as a promising technology for polarimetric weather radar measurements. In particular, the ability of PARs to synthesize imaging beams with minimal sensitivity losses is becoming increasingly crucial for achieving the high-temporal resolution requirements. This paper introduces a novel phase-only beam pattern synthesis method using the Non-Uniform Rational B-Spline (NURBS) parameterization scheme. Based on a genetic algorithm optimization, it generates a phase distribution to excite the array and produce a desired beam shape. The proposed NURBS scheme is compared to previously used Bézier parameterization scheme. An S-band, 64-element uniform linear array (ULA) PAR was constructed to evaluate the performance of the NURBS scheme. Preliminary results show that the NURBS phase parameterization scheme can be used to synthesize phase weights for real-world PARs. Multiple metrics are used to evaluate the performance of the suggested parameterization scheme, such as half-power beamwidth and peak sidelobe levels. Results suggest that the NURBS scheme performs better than the Bézier scheme for synthesizing phase-only antenna patterns.

Index Terms—phased array radar, antenna pattern synthesis, weather radar, genetic algorithm, digital radar.

I. INTRODUCTION

Phased Array Radars (PARs) are a rapidly maturing technology for polarimetric weather radar observations [1]. NOAA has recently shown an increased interest in replacing the Weather Surveillance Radar Network (WSR-88D) with rotating PARs [2–4]. As a result, the need for phase-only pattern synthesis for PARs focusing on weather observations will increase significantly. PARs can electronically steer the radar beam and generate synthesized beam patterns using *radar imaging* and other advanced methods [5]. Traditionally, antenna beam patterns are generated using amplitude and phase tapers; however, another way to generate these patterns

is through phase-only excitation with uniform amplitude excitation. Phase-only beam pattern synthesis allows for high-temporal resolution observations with minimal sensitivity loss.

Recent advancements in mobile rotating PARs at the University of Oklahoma (OU) Advanced Radar Research Center (ARRC) have two upcoming rotating weather PARs that use phase-only excitations to produce imaging antenna patterns. The two radars include the S-band, mobile, all-digital, polarimetric Horus radar, [6] and the C-Band mobile Polarimetric Atmospheric Imaging Radar (PAIR) [7]. These PARs have solid-state transmitters with relatively low power budgets; thus, a phase-only solution is needed to ensure high sensitivity when spoiled beam patterns are used to achieve high-temporal resolution observations. Spoiled beams for fast volumetric scans have been used for weather observations in radars such as the Advanced Technology Demonstrator (ATD) [8]. However, pattern synthesis methods for weather PARs with element-wise phase and amplitude control have not been widely available to the weather radar community.

This paper advances the research in this field by using a genetic algorithm optimization to produce phase-only pattern synthesis weights for spoiled beams using a new parameterization scheme. First, the Non-Uniform Rational B-Spline (NURBS) and Bézier phase parameterization schemes are characterized. Then, the optimization framework, Quality Metrics, and beam pattern envelope are defined. Subsequently, the performance of the proposed Non-Uniform Rational B-Spline (NURBS) scheme is compared to the previously investigated scheme based on Bézier curves [9, 10]. Next, the proposed NURBS scheme is evaluated using the generated phase distribution on an S-band, 64-element, uniform linear array (ULA). Finally, initial results suggest that the NURBS phase parameterization scheme outperforms the Bézier parameterization scheme.

II. PATTERN SYNTHESIS METHOD

Active PARs with phase and magnitude control at the element level can synthesize antenna radiation beam patterns on transmission and/or reception. With the capability of designing custom beam patterns, PARs can produce a variety of beams that can increase temporal data resolution when coupled with digital beamforming (DBF). However, a spoiled imaging beam supports collection of high temporal resolution data at the price of higher sidelobe levels, wider two-way half-power beamwidth, and reduced sensitivity. Therefore, to minimize sensitivity loss when using spoiled transmit beams, it is desirable to use phase-only beamforming weights to synthesize them. Although many solutions exist [10–14] to the phase-only synthesis problem, this work is the first to use NURBS to parameterize the array excitation phase.

The array factor of a Uniform Linear Array (ULA) PAR can be computed as,

$$AF(\theta, \phi) = \sum_{m=1}^M w_m e^{j\alpha_m} e^{-jm\psi_x} \quad (1)$$

where w_m , α_m are the magnitude and phase weights, and M is the number of elements in the ULA. The phase term $\psi_x = kd_x \sin(\theta) \cos(\phi)$, where $k = 2\pi/\lambda$ is the wavenumber, λ is the wavelength and d_x is the spacing in x and θ/ϕ are the steering angles in azimuth and elevation. For phase-only synthesis, we set $w_m = 1 \forall m$ and search for the best α_m .

An approximation of the one-way array pattern can be computed by combining the embedded element pattern and array factor [15],

$$F(\theta, \phi) = F_e(\theta, \phi) |AF(\theta, \phi)|^2 \quad (2)$$

where $F_e(\theta, \phi)$ represents the embedded element pattern in one polarization and $AF(\theta, \phi)$ is the array factor. In this paper only the horizontal polarization is considered.

Search spaces resulting from phase-only array-pattern synthesis can be vast and require significant computation time to find a solution even with advanced global search algorithms such as the genetic algorithm and particle swarm. Therefore, a phase parameterization scheme is needed to reduce the search space and the computation time required to find a desired array pattern. Furthermore, these parameterization schemes ensure smooth phase changes from each PAR element to the next. This paper compares phase parameterization schemes using NURBS curves and Bézier curves.

A. NURBS Parameterization

Non-uniform rational basis spline curves are smooth parameterization curves that use basis splines (B-splines). Three components define NURBS curves: order, weighted control points, and knot vector. This paper is only concerned with cubic NURBS curves. Furthermore, the control points of the NURBS curves used in this paper are weighted uniformly, and the knot vector uses the popular “average” method suggested by DeBoor to avoid singularities when globally interpolating. [16]

The general form of NURBS curves is:

$$C(u) = \sum_{i=1}^k R_{i,n}(u) \mathbf{P}_i \quad (3)$$

With \mathbf{P}_i representing control point weighting, k is the the number of control points, and $R_{i,n}(u)$ represent the rational basis functions,

$$R_{i,n}(u) = \frac{N_{i,n}(u)w_i}{\sum_{j=1}^k N_{j,n}(u)w_j} \quad (4)$$

where $N_{i,n}(u)$ and $N_{j,n}(u)$, are the B-spline basis function used for NURBS curve generation. An example set of phase weights generated using NURBS is shown in Fig. 1a.

B. Bézier Parameterization

A Bézier curve is a smooth parameterized curve of class C^1 that uses Bernstein polynomials as a basis. A generalized Bézier Curve [17] has the following form:

$$\mathbf{B}(t) = \sum_{i=0}^n b_{i,n}(t) \mathbf{P}_i, \quad 0 \leq t \leq 1. \quad (5)$$

In eq. (5), term \mathbf{P}_i represents the control points of the Bézier curve, and the term $b_{i,n}(t)$ represents the Bernstein basis function of degree n and has the form:

$$b_{i,n}(t) = \binom{n}{i} t^i (1-t)^{n-i}, \quad i = 0, \dots, n \quad (6)$$

where $\binom{n}{i}$ are the binomial coefficients.

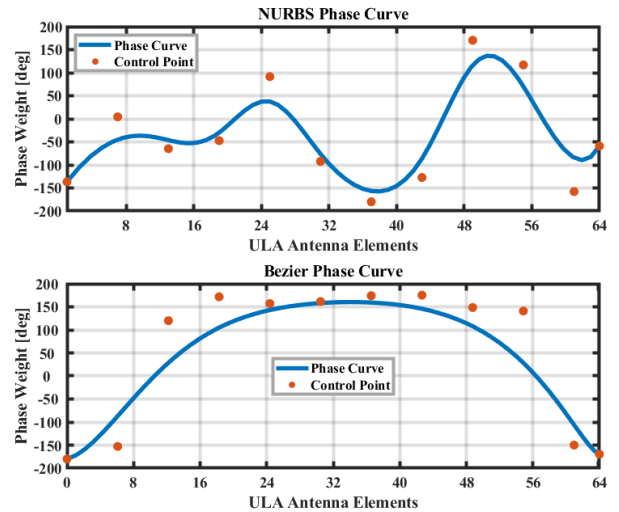


Fig. 1. Example set of phase weights generated by NURBS and Bézier parameterizations with a spacing of one control point (indicated by the red dots) every six elements.

It is important to note that depending on the number of antenna elements and control points, Bézier curves generated using the Bernstein polynomials do not result in any numerical instability. If more complex Bézier curves or Bézier patches (2-D Bézier surfaces) are needed, it may be beneficial to use

de Casteljau's Algorithm to ensure numerically stable Bézier curves or Bézier patches [17]. An example set of phase weights generated using Bézier Curves is shown in Fig. 1b.

III. OPTIMIZATION FRAMEWORK

This paper uses the genetic algorithm in conjunction with one of the parameterization schemes presented to search for phase weights that synthesize spoiled beams to best fit a desired power envelope function $E(\phi)$ and minimize the synthesis efficiency. The synthesis efficiency is the ratio of the spoiled imaging beam gain and the pencil beam gain. The synthesis efficiency metric quantifies the gain loss due to the synthesis method. Likewise, the envelope function controls the 3 dB beamwidth of the spoiled beam and the expected sidelobe levels along the azimuthal axis. The optimization problem is formulated as follows,

$$\min_{\alpha_m \in [0, 2\pi], \psi_x \in [-\pi/2, \pi/2]} F_F \quad (7)$$

subject to $w_m = 1$

where F_F is the fitness function, w_m is the magnitude weight for the antenna elements, α_m is the phase weights for the antenna elements, and ψ_x is the spoiled beam's steering angle.

We define the fitness function as a linear combination of five terms with two scaling coefficients, a and b , to ensure that all the terms in the fitness function are on the same order of magnitude. The fitness function F_F , is defined as,

$$F_F = a \times \sigma_F + M_E + I_C + b \times \rho_F + M_L \quad (8a)$$

where σ_F is the standard deviation of the the synthesized pattern's mainlobe above -3 dB with units of dB. σ_F aims to control the ripple of the mainlobe and is defined as,

$$\sigma_F = std(\{F(\phi) : F(\theta, \phi) \geq -3 \text{ dB}\}). \quad (8b)$$

M_E is defined as the integrated mainlobe spoil efficiency, which is the area of the envelope's mainlobe not filled by the synthesized pattern. This metric ensures that the shape and gain of the synthesized pattern's mainlobe closely matches the envelope's. M_E is expressed as,

$$M_E = \int_{\xi - \theta_0/2}^{\xi + \theta_0/2} [E(\phi) - B(\phi)] d\phi \quad (8c)$$

where $E(\phi)$ is the predefined envelope, $B(\phi)$ is the mainlobe of the synthesized pattern above -3 dB defined as, $B(\phi) = \{F(\theta, \phi) : F(\theta, \phi) \geq -3 \text{ dB}\}$, ξ is the steering angle of the envelope along azimuth, and θ_0 is the -3 dB beamwidth of the envelope function $E(\phi)$. Next, I_C is the integrated contamination [10], which is the area of the synthesised pattern $F(\theta, \phi)$ that exceeds the predefined envelope $E(\phi)$ which ensures that the sidelobe levels are controlled. I_C is defined as,

$$I_C = \int_{-\pi/2}^{\pi/2} \frac{\max[F(\theta, \phi), E(\phi)]}{E(\phi)} d\phi \quad (8d)$$

ρ_F is the piecewise Pearson correlation coefficient, which quantifies the symmetry of the mainlobe of the synthesized pattern and is defined as

$$\rho_F = \begin{cases} -\rho_{F_0, F_1} & \rho_{F_0, F_1} \geq 0.5 \\ 0 & \rho_{F_0, F_1} < 0.5 \end{cases} \quad (8e)$$

where ρ_{F_0, F_1} is the Pearson correlation coefficient defined as,

$$\rho_{F_0} = \frac{cov(F_0, F_1)}{\sigma_{F_0} \sigma_{F_1}}$$

where $F_0 = \{F(\theta, \phi) : \phi \leq \xi\}$, $F_1 = \{F(\theta, \phi) : \phi \geq \xi\}$ σ_{F_1} , and σ_{F_2} are the standard deviations of F_1 and F_2 . M_L is the mainlobe leakage, defined as the mean of the number of changes in concavities in the synthesized pattern outside the -3 dB beamwidth (BW) of the envelope $E(\phi)$. This fitness function term aims to penalize the optimization based on the number of "shoulders" (a change in the pattern's concavity) near the mainlobe that exceeds the envelope. M_L is defined as,

$$M_L = 10 \log_{10} \left(\frac{\sum_{i=0}^N (F''_{i,0})}{N} + \frac{\sum_{i=0}^N (F''_{i,1})}{N} + 1 \right) \quad (8f)$$

where N is the number of sample points of the pattern $F(\theta, \phi)$ along ϕ and $F''_{i,0}$ is the piecewise positive concavity of F''_0 defined as,

$$F''_{i,0} = \begin{cases} 1 & F''_0 \geq 0 \\ 0 & F''_0 < 0 \end{cases}$$

where F''_0 is,

$$F''_0 = \frac{\partial^2 F}{\partial \phi^2} \{F(\theta, \phi) : \phi \leq \xi - \theta_0/2, F(\theta, \phi) > -27 \text{ dB}\}$$

$F''_{i,1}$ is the piecewise positive concavity of F''_1 defined as,

$$F''_{i,1} = \begin{cases} 1 & F''_1 \geq 0 \\ 0 & F''_1 < 0 \end{cases}$$

and F''_1 is,

$$F''_1 = \frac{\partial^2 F}{\partial \phi^2} \{F(\theta, \phi) : \phi \geq \xi + \theta_0/2, F(\theta, \phi) > -27 \text{ dB}\}$$

Note that in eq. (8f) the +1 is a compensation term to avoid edge cases where the sum of the terms inside the logarithm is lower than 1.

With the five-value linear combination fitness function and synthesis efficiency framework in place, the optimization will generate phase weights that synthesize an antenna beam pattern that approximates the desired envelope function while minimizing the fitness function value.

IV. COMPARISON OF PARAMETERIZATION PERFORMANCE

This section compares the performance of the two parameterization schemes described in Sections II-A and II-B. We compare the performance of the parameterization schemes in two ways. First, we compare the optimization results as a function of the parameterization's control point spacing. Then, the control point spacing that resulted in the minimum fitness function value is selected as the optimal spacing for that parameterization scheme and used in the second analysis. The second analysis focuses on each parameterization's

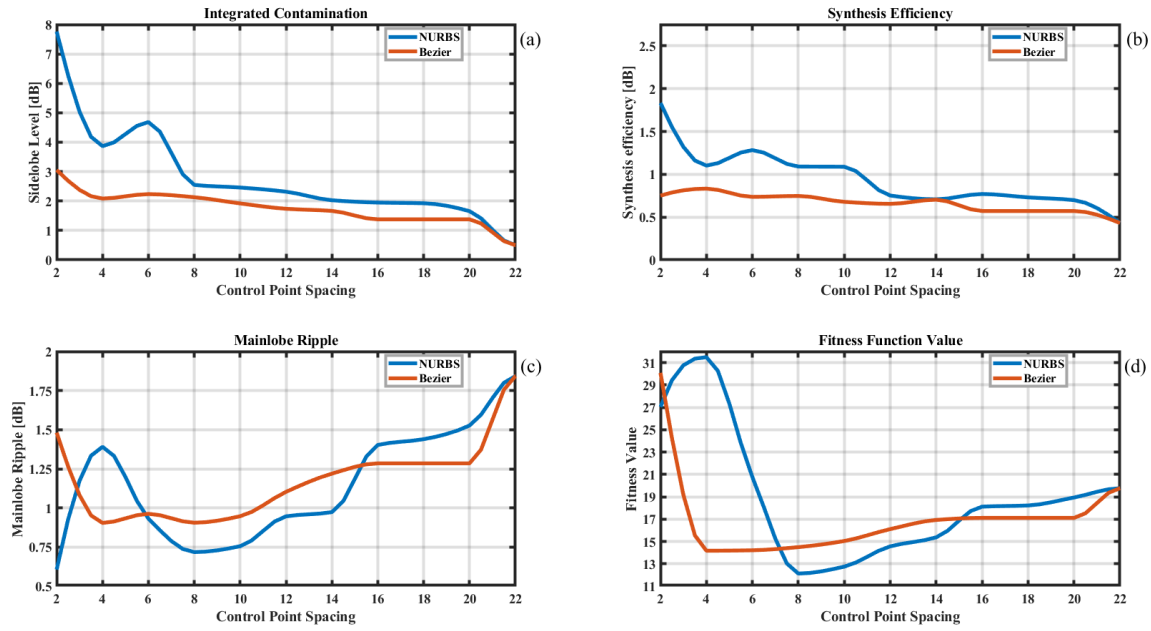


Fig. 2. Quality Metrics as a function of control point spacing: (a) Integrated Contamination, (b) Synthesis Efficiency, (c) Mainlobe Ripple, (d) Fitness Function Value.

performance as a function of steering angle in azimuth. The following four Quality Metrics (QM) are used to measure the performance of each scheme:

- Integrated Contamination (I_C)
- Synthesis Efficiency (SE)
- Mainlobe Ripple
- Fitness function value

The integrated contamination and mainlobe ripple are part of the fitness function defined in eq. (8a). The fitness function value is computed as in eq. (8a). Moreover, synthesis effi-

ciency measures the optimization's efficiency in minimizing sensitivity losses. Note that the lower the value, the better the performance for all quality metrics presented. For all performance comparisons, we used a 1-D envelope function with a beamwidth of 10° in azimuth, shown in Fig. 3. This standardized envelope function ensures fair comparisons for the NURBS and Bézier parameterization schemes.

A. Performance as a Function of Number of Control Points

We investigate the performance as a function of control point spacing for the two parameterization schemes. This allows for determining the optimal number of control points for each parameterization scheme and the lower limit on the number of control points needed before performance degradation occurs.

In this comparison, the control point spacing will range from 2 to 22 elements per control point, and the 1-D envelope will be centered at 0° degrees in azimuth, as seen in Fig. 3. The genetic algorithm optimization was run ten times for each control point spacing, and the best convergence (i.e., having the lowest fitness function value) was selected among the ten runs for analysis. Fig. 2 shows the four QMs as a function of control point spacing for the two parameterization schemes. The Bézier parameterization scheme has lower integrated contamination than the NURBS scheme for most control point spacings, as seen in Fig. 2a. Furthermore, the SE from Fig. 2b shows the Bézier parameterization scheme performing best for most of the control point spacings, while NURBS and Bézier shared the global minimum at control point spacing 22. Fig. 2c shows that the NURBS parameterization performs better than

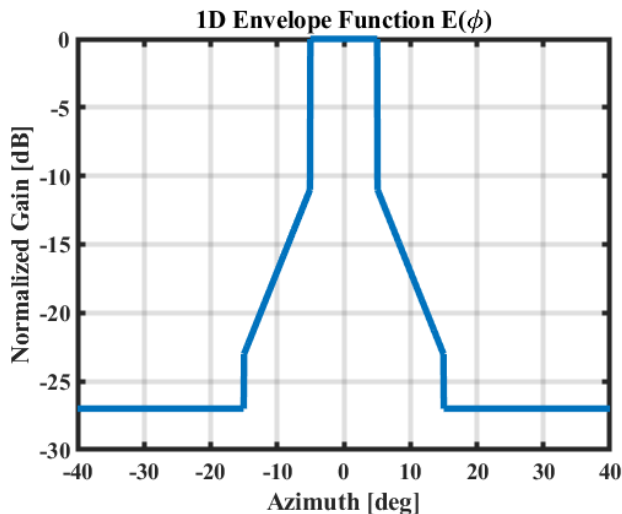


Fig. 3. 1-D Envelope Function $E(\phi)$. with 10° beamwidth, sidelobe levels of -12 dB and secondary sidelobe levels of -27 dB.

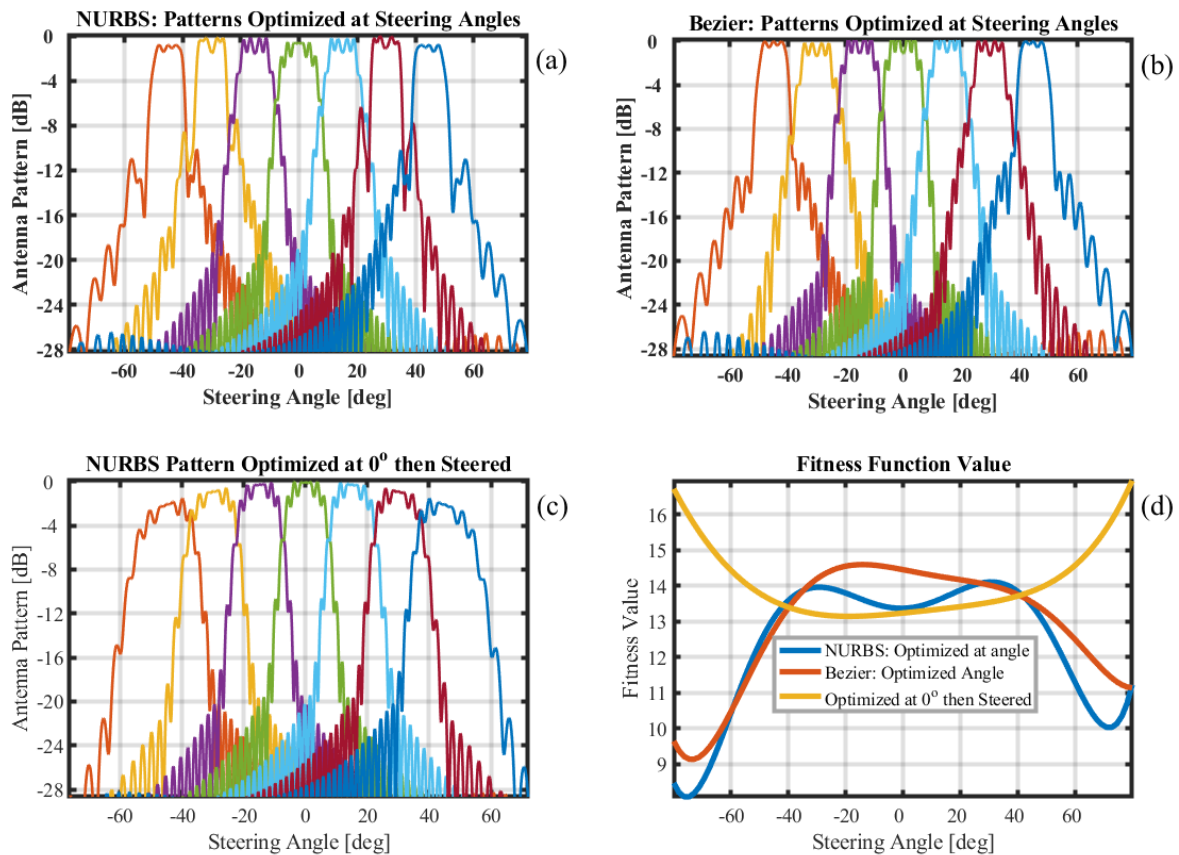


Fig. 4. Resulting synthesized patterns as a function of envelope steering angle and fitness function value: (a) NURBS optimized at steering angle, (b) Bézier optimized at steering angle, (c) Pattern optimized at broadside then electronically steered, (d) Fitness function value.

the Bézier scheme from control point spacings 6 to 14 for mainlobe ripple. In this case, NURBS has a global minimum of 0.718 dB of ripple at a control point spacing of eight and Bézier has a minimum of 0.904 dB of ripple at a control point spacing of four.

Subsequently, Fig. 2d plots the NURBS and Bézier parameterization scheme's fitness function values. The NURBS scheme has a minimum value of 12.1 at a control point spacing of eight, while the minimum value of the Bézier scheme is 14.1 at a control point spacing of four. The lower fitness function value implies that the NURBS scheme performed better than the Bézier scheme. NURBS's larger control point spacing also implies it is a more computationally efficient method because it has a smaller search space. Reductions in convergence time are noteworthy as these schemes are expanded to planar PARs with thousands of elements. To further illustrate the difference in the NURBS and Bézier parameterization schemes, Fig. 4a and Fig. 4b show the best far-field copolar patterns that the NURBS and Bézier schemes were able to synthesize. The NURBS pattern was synthesized using the phase weights generated from a control point spacing of eight, while the Bézier pattern was synthesized using the phase weights from

a control point spacing of four.

B. Performance as a Function of Steering Angle

Next, we compare optimizing a spoiled beam at a specific azimuth angle versus optimizing at broadside and then steering to the desired azimuth angle. To optimize a spoiled beam at each azimuth steering angle, we use the best Bézier and NURBS control point spacing from Section IV-A: four for Bézier and eight for NURBS. The envelope is then moved from -45° to 45° in azimuth centered at the desired steering angle, and the genetic algorithm is run ten times for each. The best out of ten convergences is selected based on the lowest fitness function value. Next, we generate a pattern at the broadside using the NURBS parameterization scheme with a control point spacing of eight, and we then electronically steer the beam from -45° to 45° in azimuth to calculate QMs at each steering angle.

The results in Fig. 4 show that optimizing spoiled beams at a steering angle regardless of parameterization type has many advantages. Two of the most notable advantages are reductions in scan loss and beam broadening coming from the embedded antenna element patterns used. Figs. 4a, 4b, and 5b also show reduced SE and beam broadening. Furthermore, in Fig. 5d, the

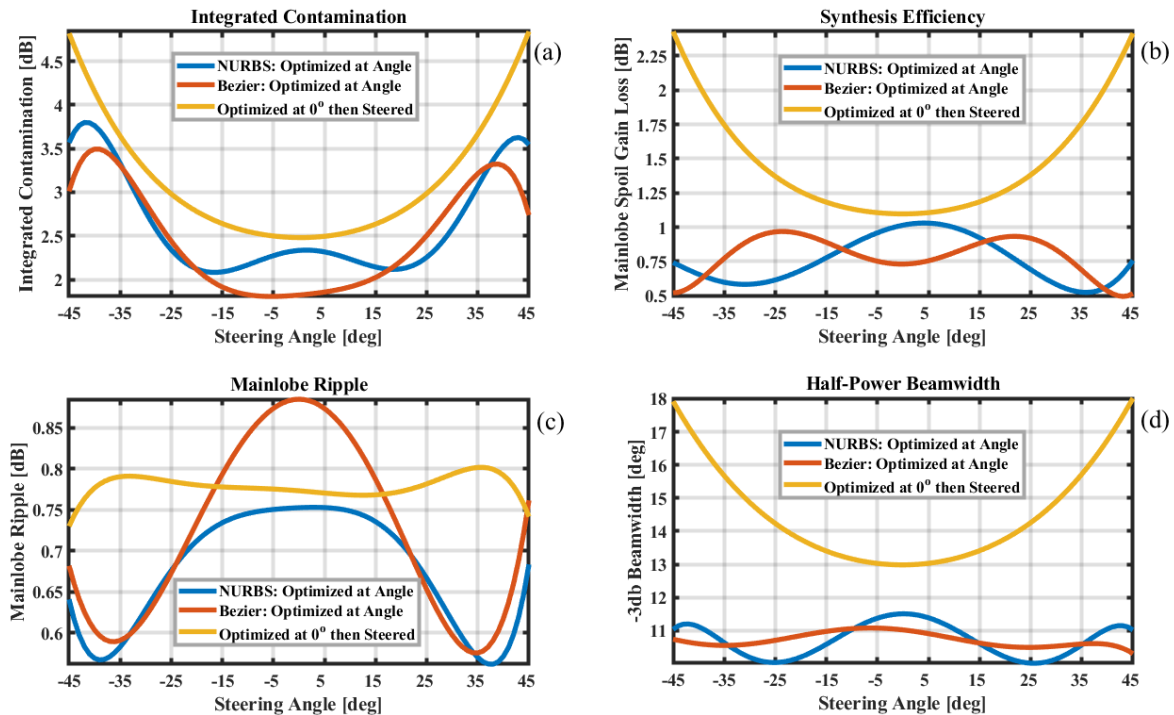


Fig. 5. (a) Integrated Contamination, (b) Synthesis Efficiency, (c) Mainlobe Ripple, (d) Half-Power Beamwidth.

half-power beamwidth, defined herein as the angular width in degrees within which the microwave radiation is greater than one-half of its peak intensity (-3 dB), shows that optimizing at a specific steering angle with either parameterization scheme will largely mitigate beam broadening. To further support this conclusion, Tab. I shows that the average beamwidth for the steered spoiled beams is 14.4941° while optimizing at a steering angle resulted in an average half-power beamwidth of 10.7206° for Bézier, and 10.7167° for NURBS. Based on these averages, optimizing at a specific steering angle regardless of the parameterization scheme results in spoiled beams with beamwidths comparable to that of the envelope. Similarly, optimizing at a steering angle improves SE, with average values of 0.7564 dB for NURBS and 0.7891 dB for Bézier, compared to the steered beam's value of 1.4690 dB. Again, this improvement is encouraging because beam broadening and scan loss are well-documented issues when electronically steering off the broadside. Finally, the average fitness score shown in Tab. I indicates that NURBS performs the best with an average fitness value of 12.3855 and that both

NURBS and Bézier's fitness function values are less than that of the steered spoiled beams.

V. 64 ELEMENT ULA SYNTHESIZED BEAM PATTERN

Actual implementation and testing of the phase weights generated by the proposed NURBS phase parameterization scheme was achieved with a 64-element, S-band, dual-polarization uniform linear array (ULA) constructed, operating at a frequency of 3 GHz. While the ULA is a dual-polarization PAR, we only used the vertical polarization to validate the synthesized beam patterns. The element spacing for the ULA is $\lambda/2 = 50.8$ mm, as seen in Fig. 6. The 64-element ULA is controlled by a set of 8 phase and amplitude control (PAC) boards, allowing element-wise signal and TX/RX control. The PAC boards are wirelessly controlled with a Raspberry Pi over a local network. For near-field array calibration and measurements, we used the Universal Robotics UR-10 robotic arm with an attached 3×3 array (center element excited, others terminated) at a distance of 4λ or 40.64 cm from the face of the ULA, shown in Fig. 2. 7. Further, using the UR-10

Summary of the Performance as a Function of Steering Angle					
Parameterization Schemes	Fitness Average	Integrated Contamination Average	Ripple Average	SE Average	Half-Power Beamwidth Average
Bézier	12.9028	2.4782 dB	0.7208 dB	0.7891 dB	10.7206°
NURBS	12.3855	2.6256 dB	0.6751 dB	0.7564 dB	10.7167°
Steered	14.0561	3.1438 dB	0.7783 dB	1.4690 dB	14.4941°

TABLE I

NOTE: 'STEERED' REFERS TO THE PATTERN OPTIMIZED AT 0° AND THEN STEERED ELECTRONICALLY IN AZIMUTH.

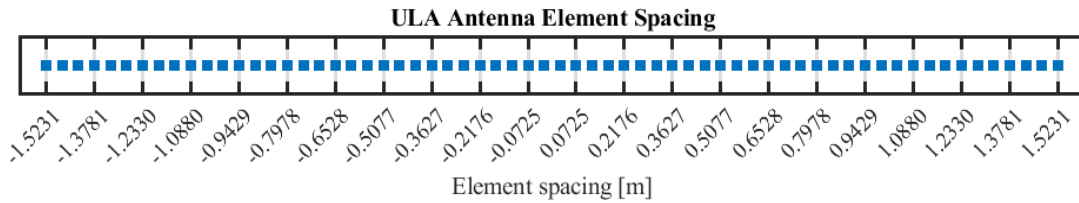


Fig. 6. ULA antenna element spacing.

robot minimizes calibration errors and improves measurement stability.

To evaluate synthesized patterns from the ULA, the UR-10 robot and probe are used to measure the near-field pattern. Due to the large size of the ULA, fields are measured in two parts. First, we measured each half of the array independently (left and right). Then, we coherently summed these two measurements to form the final near-field pattern. Finally, we perform the near-field to far-field transformation defined in [18] to compute a co-polar far-field patterns. Fig. 8 shows the simulated and measured far-field patterns. We used the phase coefficients generated by the NURBS broadside pattern in Fig. 4a. The simulated pattern in Fig. 8 is very similar to the synthesized pattern. However, the sidelobe levels and mainlobe ripple do not agree very well. These mismatches are likely due to the open environment in which the measurements were taken. Therefore, changes to the methodology for future measurements should be made. Three promising solutions would be either increasing the SNR of the ULA, decreasing the near-field probe's distance to the face of the ULA, or increasing the near-field sample spacing.

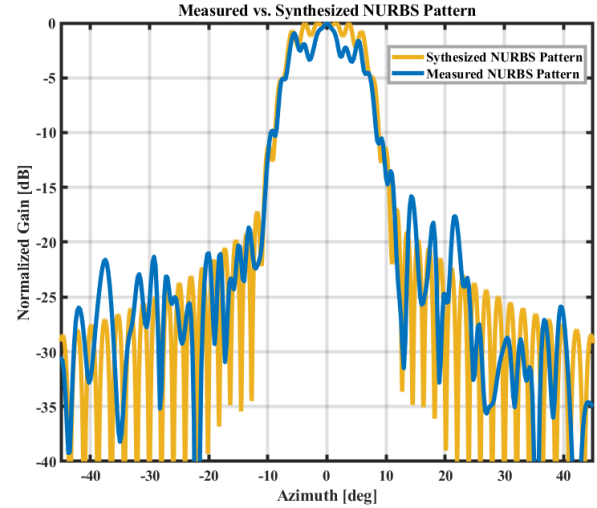


Fig. 8. Measured and simulated far-field ULA patterns for NURBS parameterization scheme with a spacing of one control point every eight elements. Note that the same phase coefficients are used for generating both the measured and simulated patterns.

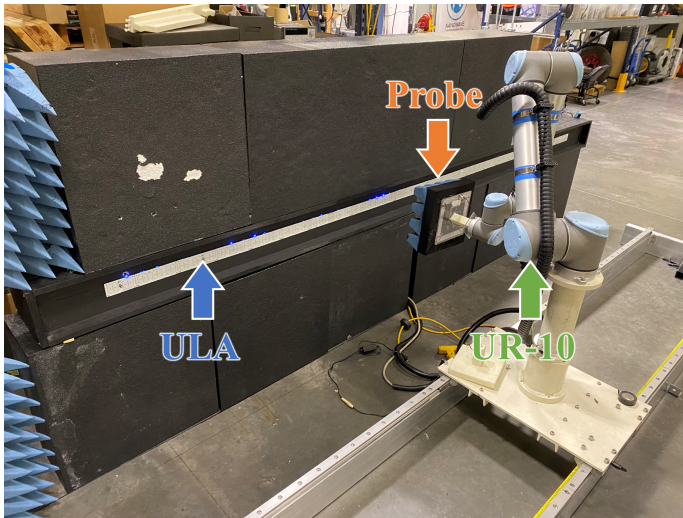


Fig. 7. ULA near-field calibration and measurement setup using antenna probe and UR-10 robot.

VI. CONCLUSION

This paper presents progress towards an optimization method for synthesizing phase-only antenna beam patterns

using phase parameterization schemes to improve the resolution and gain of synthesized patterns, the convergence time, and to ensure smooth element-to-element phase transitions. We use the genetic algorithm solver to efficiently search for a global optimum. The optimization is driven by two factors. The 1-D envelope function, which controls the shape, the beamwidth, and the sidelobe levels of the synthesized patterns; and the fitness function that controls the synthesized pattern's integrated contamination, mainlobe ripple, mainlobe spoil gain efficiency, piecewise Pearson correlation coefficient, and mainlobe leakage.

Preliminary results suggest that the proposed NURBS parameterization scheme can be used to generate phase-only weights for spoiled imaging beams. It outperforms the Bézier scheme for all metrics except integrated contamination when optimized at specific steering angles. An important finding is that synthesizing spoiled beams at a specific steering angle can significantly reduce beam broadening and scan losses for both parameterization schemes. Finally, the phase weights generated from the NURBS parameterization scheme were implemented into a ULA to validate actual performance of the derived phase weights. An essential next step is to expand the NURBS parameterization scheme to 2-D NURBS surfaces for planar PARs.

ACKNOWLEDGMENT

This work is supported by NOAA/Office of Oceanic and Atmospheric Research under NOAA-University of Oklahoma Cooperative Agreement #NA21OAR4320204, U.S. Department of Commerce. Any opinions, findings, and conclusions or recommendations expressed in this material are those of the author(s), and do not necessarily reflect the views of NOAA. The authors would like to thank the ARRC leadership and the ARRC engineers for their support in the design & development efforts. Special thanks to ARRC engineers Matthew Herndon and Hong Pan for helping with the PAC boards and ARRC student Alexis Oblitas Mantilla for helping with the ULA calibration and construction.

REFERENCES

- [1] D. S. Zmic *et al.*, "Agile-Beam Phased Array Radar for Weather Observations," *Bull. of the American Meteorological Society*, vol. 88, no. 11, pp. 1753–1766, Nov. 2007. DOI: 10.1175/BAMS-88-11-1753.
- [2] NOAA/NWS, "Radar Functional Requirements," Tech. Rep., 2015, Available: https://roc.noaa.gov/WSR88D/PublicDocs/NOAA_Radar_Functional_Requirements_Final_Sept%202015.pdf.
- [3] K. Hondl and M. Weber, "NOAA's Meteorological Phased Array Radar Research Program," in *2019 IEEE International Symposium on Phased Array System Technology (PAST)*, 2019, pp. 1–6. DOI: 10.1109/PAST43306.2019.9020994.
- [4] D. Schwartzman, "Signal Processing Techniques and Concept of Operations for Polarimetric Rotating Phased Array Radar," Available at <https://hdl.handle.net/11244/326580>, Ph.D. dissertation, The University of Oklahoma, Norman, OK, USA, 2020.
- [5] R. D. Palmer *et al.*, "A Primer on Phased Array Radar Technology for the Atmospheric Sciences," *Bulletin of the American Meteorological Society*, 2022, Under review.
- [6] R. D. Palmer, C. J. Fulton, J. Salazar, H. Sigmarsson, and M. Yeary, "The "Horus" Radar—An All-Digital Polarimetric Phased Array Radar for Multi-Mission Surveillance," in *99th American Meteorological Society Annual Meeting*, AMS, 2019.
- [7] T. Yu, J. Salazar, D. Schwartzman, C. Fulton, R. Palmer, and H. Bluestein, "A Shared Mobile C-Band Polarimetric Atmospheric Imaging Radar (PAIR)," 2022.
- [8] D. Schwartzman, S. M. Torres, and T.-Y. Yu, "Distributed Beams: Concept of Operations for Polarimetric Rotating Phased Array Radar," *IEEE Transactions on Geoscience and Remote Sensing*, vol. 59, no. 11, pp. 9173–9191, 2021. DOI: 10.1109/TGRS.2020.3047090.
- [9] D. Schwartzman, R. Palmer, T.-Y. Yu, R. Reinke, and F. Nai, "A Pattern Synthesis Method for Polarimetric Weather Observations with the All-Digital Horus Phased Array Radar," in *102nd American Meteorological Society Annual Meeting*, AMS, 2022.
- [10] D. Schwartzman, J. D. D. Díaz, J. L. Salazar-Cerreño, T.-Y. Yu, R. D. Palmer, and M. S. McCord, "A Hybrid Antenna Pattern Synthesis Method for the Polarimetric Atmospheric Imaging Radar (PAIR)," in *2022 IEEE Radar Conference (RadarConf22)*, 2022, pp. 01–06. DOI: 10.1109/RadarConf2248738.2022.9764359.
- [11] J. Liang, X. Fan, W. Fan, D. Zhou, and J. Li, "Phase-Only Pattern Synthesis for Linear Antenna Arrays," *IEEE Antennas and Wireless Propagation Letters*, vol. 16, pp. 3232–3235, 2017. DOI: 10.1109/LAWP.2017.2771380.
- [12] D. P. Scholnik, "A Parameterized Pattern-Error Objective for Large-Scale Phase-Only Array Pattern Design," *IEEE Transactions on Antennas and Propagation*, vol. 64, no. 1, pp. 89–98, 2016. DOI: 10.1109/TAP.2015.2500239.
- [13] W. M. Dorsey and D. P. Scholnik, "A hybrid global-local optimization approach to phase-only array-pattern synthesis," in *2015 IEEE Radar Conference (RadarCon)*, 2015, pp. 1417–1422. DOI: 10.1109/RADAR.2015.7131217.
- [14] G. Buttazzoni and R. Vescovo, "An Efficient and Versatile Technique for the Synthesis of 3D Copolar and Crosspolar Patterns of Phase-Only Reconfigurable Conformal Arrays With DRR and Near-Field Control," *IEEE Transactions on Antennas and Propagation*, vol. 62, no. 4, pp. 1640–1651, 2014. DOI: 10.1109/TAP.2014.2308319.
- [15] R. J. Mailloux, *Phased array antenna handbook*. Artech house, 2017, pp. 109–153.
- [16] L. Piegl and L. A. Piegl, *The NURBS Book by Les Piegl, Wayne Tiller*. eng, Second edition..., ser. Monographs in visual communication. Berlin, Heidelberg: Springer Berlin Heidelberg, 1997, pp. 117–141.
- [17] C. T. Loop and T. D. DeRose, "A Multisided Generalization of BéZier Surfaces," *ACM Trans. Graph.*, vol. 8, no. 3, pp. 204–234, Jul. 1989. DOI: 10.1145/77055.77059.
- [18] C. A. Balanis, *Antenna Theory: Analysis and Design*. John Wiley & Sons, 2015, pp. 319–348.